Applied Physics Letters

Basic physical properties of cubic boron arsenide

Cite as: Appl. Phys. Lett. **115**, 122103 (2019); https://doi.org/10.1063/1.5116025
Submitted: 26 June 2019 . Accepted: 09 August 2019 . Published Online: 17 September 2019

Joon Sang Kang, Man Li, Huan Wu, Huuduy Nguyen, and Yongjie Hu

AIP Publishing

Applied Physics Letters ARTICLE scitation.org/journal/apl

Basic physical properties of cubic boron arsenide

Cite as: Appl. Phys. Lett. **115**, 122103 (2019); doi: 10.1063/1.5116025
Submitted: 26 June 2019 · Accepted: 9 August 2019 ·
Published Online: 17 September 2019

Joon Sang Kang, Man Li, Huan Wu, Huuduy Nguyen, and Yongjie Hu[a)]

AFFILIATIONS

School of Engineering and Applied Science, University of California, Los Angeles (UCLA), Los Angeles, California 90095, USA

[a)]Author to whom correspondence should be addressed: yhu@seas.ucla.edu

ABSTRACT

Cubic boron arsenide (BAs) is an emerging semiconductor material with a record-high thermal conductivity subject to intensive research interest for its applications in electronics thermal management. However, many fundamental properties of BAs remain unexplored experimentally since high-quality BAs single crystals have only been obtained very recently. Here, we report the systematic experimental measurements of important physical properties of BAs, including the bandgap, optical refractive index, elastic modulus, shear modulus, Poisson's ratio, thermal expansion coefficient, and heat capacity. In particular, light absorption and Fabry–Pérot interference were used to measure an optical bandgap of 1.82 eV and a refractive index of 3.29 (657 nm) at room temperature. A picoultrasonic method, based on ultrafast optical pump probe spectroscopy, was used to measure a high elastic modulus of 326 GPa, which is twice that of silicon. Furthermore, temperature-dependent X-ray diffraction was used to measure a linear thermal expansion coefficient of 3.85×10^{-6} K^{-1}; this value is very close to prototype semiconductors such as GaN, which underscores the promise of BAs for cooling high power and high frequency electronics. We also performed *ab initio* theory calculations and observed good agreement between the experimental and theoretical results. Importantly, this work aims to build a database (Table I) for the basic physical properties of BAs with the expectation that this semiconductor will inspire broad research and applications in electronics, photonics, and mechanics.

Heat dissipation is a critical technology issue for modern electronics and photonics.[1–5] A key challenge and urgent need for effective thermal management is to discover new materials with ultrahigh thermal conductivity for dissipating heat from hot spots efficiently, thereby improving device performance and reliability.[6–10] Options to address this challenge with conventional high thermal conductivity materials, such as diamond and cubic boron nitride, are very limited;[11–13] their high cost, slow growth rate, degraded crystal quality, combined with the integration challenge with semiconductors, given chemical inertness and large mismatch in lattice and thermal expansion, make them far from optimal candidates. Carbon-based nanomaterials, such as graphene and carbon nanotubes, are limited by their intrinsic anisotropic thermal conductivity and performance degradation due to ambient scattering despite the fact that individual materials can have high thermal conductivity.[14] A recent *ab initio* theory calculation has predicted new boron compounds with high thermal conductivity stemming from the fundamental vibrational spectra.[15–17] Although the early growth was reported in the 1950s,[18–23] obtaining high-quality crystals of these materials with minimal defects has proven challenging and was only achieved very recently.[6–9] Our recent study[7] reports the successful synthesis of single-crystal BAs with nondetectable defects, along with the measurement of a record-high thermal conductivity of 1300 W/mK, a value which is beyond that of most common semiconductors and metals. Thus, BAs is a promising new semiconductor that could potentially revolutionize the current technology paradigms of thermal management and possibly extend the semiconductor roadmap. However, many of the basic physical properties of BAs have yet to be explored experimentally. Here, we report the systematic experimental study of our chemically synthesized high-quality BAs crystals, including the measurement of basic BAs characteristics such as the bandgap, optical refractive index, sound velocity, elastic modulus, shear modulus, Poisson's ratio, thermal expansion coefficient, and heat capacity.

High-quality BAs single crystals (Fig. 1) were synthesized by the chemical vapor transport reaction as described in our previous work.[7] BAs has a zinc-blended face-centered crystal structure with an $F\bar{4}3m$ space group, where boron and arsenic atoms interpenetrate each other and are covalently bonded with a lattice constant of 4.78 Å. The synthetic BAs crystals, characterized by high-resolution scanning transmission electron microscopy, show an atomically resolved lattice.

We report the experimental measurement of the optical bandgap (E_g) of BAs. E_g is a major factor that determines the optical absorption and electrical transport in a solid. However, owing to the synthesis challenge to obtain high-quality crystals until recently,[7] the E_g of bulk BAs remained inconclusive with theoretically calculated values varying from 0.67 to 5.5 eV.[24–30] Here, we measured the light absorption of BAs single crystals to determine E_g using ultraviolet–visible spectroscopy.

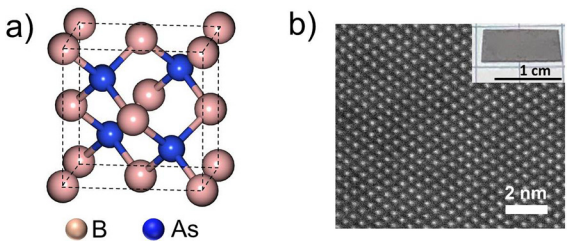

FIG. 1. Cubic BAs crystals. (a) Unit cell structure of BAs; (b) high-resolution scanning transmission electron microscopy image of BAs with the ⟨110⟩ zone axis. Inset: optical image of a BAs thin film sample.

The transmission spectrum of BAs was collected by scanning light wavelengths with photon energy from 1.5 to 2.2 eV, following the Beer–Lambert law,

$$\frac{I}{I_0} = e^{-\alpha d}, \tag{1}$$

where I and I_0 are the transmitted light and the intensity of incident light, respectively, and α and d are the absorption coefficient and the thickness of the sample crystal, respectively. Figure 2(a) shows the absorption measurement data. As an indirect bandgap semiconductor, the band edge absorption of BAs was determined by[31]

$$\alpha \propto \left(h\nu - E_g \pm \hbar\Omega\right)^2, \tag{2}$$

where h and ν are the Planck constant and light frequency, respectively. Equation (2) indicates a threshold in the absorption close to E_g, but with a small $\hbar\Omega$ difference due to the contribution of phonons during the light absorption process, as required by momentum conservation. The absorption data plot of $\alpha^{\frac{1}{2}}$ vs $h\nu$ fits well onto a straight line, which confirms Eq. (2) and enables the extrapolation of $E_g \sim 1.82$ eV. Note that E_g could be slightly shifted due to the absorption or emission of phonons, whose energies at the X point are 0.02 ∼ 0.04 eV for transverse acoustic (TA) and longitudinal acoustic (LA) branches. In addition, the experimental curve shows a tail extending down to about 1.5 eV, which is caused by the absorption of high-energy phonons or multiphonons.

We also measured the refractive index of BAs. The refractive index (n) is a key dimensionless parameter for photonic applications which describes how fast light propagates through the material, but was unknown for BAs so far. Theoretical refractive indexes of BAs appearing in the recent literature[28,30,32,33] have different values, possibly due to variations in pseudopotentials[28,30,32] or empirical relationships. Here, we directly measured n by Fabry–Pérot interference. When light passes through a BAs crystal [inset of Fig. 2(b)], the top and bottom surfaces can serve as two parallel reflecting mirrors. The transmission spectrum measured as a function of wavelength from 657 to 908 nm exhibits large resonance oscillations [Fig. 2(b)]. n can be extracted from the following equation under normal light incidence:[34,35]

$$n = \frac{M\lambda_1\lambda_2}{2(\lambda_1 - \lambda_2)d}, \tag{3}$$

where M is the number of fringes between the two extrema (M = 1 for consecutive maxima) and λ_1 and λ_2 are the corresponding light wavelength between fringes. The refractive index of BAs was measured as

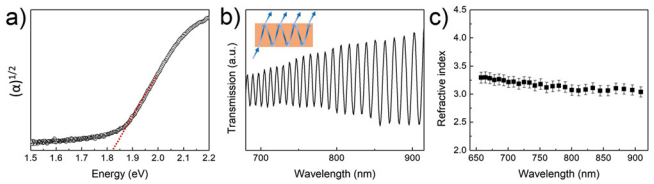

FIG. 2. Optical properties of BAs. (a) Bandgap measurement from light absorption experiments. The absorptivity is plotted vs the photon energy of a 55 μm thick BAs sample; (b) refractive index measurement from a Fabry–Pérot interference experiment: the optical transmission measured on a 8.79 μm thick BAs sample shows strong oscillations due to resonances from the light reflected by the top and bottom sample surfaces (inset); and (c) wavelength dependent refractive index of BAs.

n = 3.29 to 3.04 with increased optical wavelengths from 657 to 908 nm and plotted in Fig. 2(c), which is close to that of prototyped optoelectronic materials, such as GaP (3.2 at 900 nm)[36] and GaAs (3.7 at 876 nm).[37]

Next, we measured the basic mechanical properties of BAs, including elastic modulus, shear modulus, sound velocity, and Poisson's ratio. The stresses and strains of a material are connected by Hooke's spring law

$$\sigma_{ij} = C_{ijkl}\varepsilon_{kl}, \tag{4}$$

where σ, C, and ε are the stress, stiffness, and strain, respectively. In general, for anisotropic materials, C_{ijkl} is a fourth-order tensor with 81 components.[38,39] Under the symmetry and Voigt notation,[40] the stiffness tensor can be simplified to 36 components. For cubic symmetry materials, such as BAs, only 3 constitutive components—C_{11}, C_{12}, and C_{44}—are independent. They are closely related to the sound velocities as discussed below.

To measure the stiffness of BAs, we first performed picosecond ultrasonic measurements[41] to determine sound velocity using pump-probe ultrafast optical spectroscopy[42–45] [Fig. 3(a)]. In this setup, a thin metal layer (aluminum) is deposited on the BAs surface to serve as the optical transducer and a picosecond laser pump generates a longitudinal acoustic wave that penetrates into the BAs sample, travels across it, reflects back, and creates sound echoes. The sound echoes are detected by a probe pulse laser with a controlled subpicosecond stage delay [Fig. 3(b)]. The time delay (Δt_{echo}) between echoes is measured and contributed to by the round trip of the acoustic wave in the BAs film with a given thickness (d), thus determining the sound velocity,

$$v_{LA} = \frac{2 \cdot d}{\Delta t_{echo}}. \tag{5}$$

For example, we prepared a BAs thin film slab along the (111) orientation using a focused ion beam (FIB) [inset of Fig. 3(b)] and the room temperature $v_{LA,111}$ is 8150 ± 450 m/s. We also measured the temperature dependence from 80 to 500 K [Fig. 3(c)], indicating a slight decrease in sound velocity with increased temperature. Note that the stiffness C_{44} can be linked with $v_{LA,111}$, C_{11}, and C_{12} with the following formula:[46]

$$C_{44} = \frac{\left(3\rho v_{LA,111}{}^2 - C_{11} - 2C_{12}\right)}{4}, \tag{6}$$

where the mass density ρ is 5.22 g/cm^{3}for BAs.[7] Since C_{11} and C_{12} can be linked by[38] $C_{12} = \frac{3B - C_{11}}{2}$, where B is the bulk modulus reported as

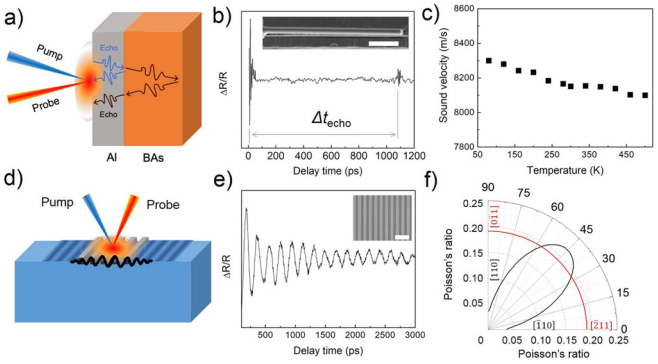

FIG. 3. Mechanical properties of BAs. (a) Schematic of the picosecond ultrasonic measurement process. (b) Picosecond acoustic data: the sound echoes indicate a round trip of the acoustic wave generated inside the BAs sample. The inset shows a thin film (4.37 μm) of BAs prepared with a focused ion beam in the (111) plane; (c) temperature dependent sound velocity of BAs; (d) schematic of the surface acoustic wave (SAW) measurement using ultrafast pump-probe spectroscopy; (e) the detection signal as a function of delay time shows periodic oscillations corresponding to the propagation of a SAW. The inset shows a fabricated metal pattern for the SAW measurement using e-beam lithography. The scale bar is 1 μm; and (f) the measured Poisson's ratio of BAs on the (100) plane (black line) and (111) plane (red line).

148 GPa,[47,48] C_{11} cancels out in Eq. (6) leaving a relationship between C_{44} and $v_{LA,111}$. Therefore, from these results, the stiffness C_{44} is determined to be 149 GPa. The transverse acoustic velocity along ⟨100⟩ is $v_{TA} = \sqrt{\frac{C_{44}}{\rho}} = 5340 \pm 510$ m/s.

To obtain the stiffness C_{11}, we measured surface acoustic waves (SAWs)[49,50] [Fig. 3(d)]. Periodic metal lines (with a period of L) were fabricated on the surface of BAs samples in alignment with the desired crystal directions using electron beam lithography[51] and heated up by a pulsed laser to generate periodic thermal strains that partially pass through the sample to form SAWs [Fig. 3(d)].[44,52,53] The SAW propagating along the BAs surface and detected by a laser probe shows strong periodic oscillations with a time periodicity of Δt_{SAW} in the ultrafast time domain [Fig. 3(e)], which measures the SAW velocity. For example, for the main top crystal surface in the (111) orientation, the SAW velocity was measured as $v_{SAW} = L/\Delta t_{SAW} = 4320 \pm 120$ m/s, which is used to extract the C_{11} of BAs as discussed below.

In general, the bulk wave equation for the displacement in a perfectly elastic and anisotropic medium can be written as

$$C_{ijkl}\frac{\partial^2 u_k}{\partial x_l \partial x_j} = \rho\frac{\partial^2 u_i}{\partial t^2}, \tag{7}$$

where u_i are the displacement components along the Cartesian axes x_i to which the stiffness tensor C_{ijkl} is referred. ρ is the mass density and the Einstein summation is implied. For bulk waves, the solutions of Eq. (7) are plane waves. However, for SAWs, these solutions represent the propagation modes of elastic energy along the free surface of a half-space, and their displacement amplitudes decay exponentially with depth so that most energy is concentrated within a wavelength distance below the surface.[50,54] When a combination coefficient (A) for each wave component is used to consider the direction-dependent free propagation, space confinement, and amplitude decays, respectively, the solution for SAWs can be written as linear combinations[50]

$$u_i = \sum_m A^{(m)} U_j^{(m)} \exp(ik(l_i x_i - v_{SAW} \cdot t)), \tag{8}$$

where k, U_j, δ_{ij}, and l are the wave vector, amplitude, Kronecker delta, and directional vector, respectively. The solution of equation (8) can be determined by substituting the wave forms of Eq. (8) into Eq. (7), which leads to the Christoffel equation,

$$\left[k^2 l_i l_l c_{ijkl} - \rho\omega^2 \delta_{ij}\right][U_i] = 0, \tag{9}$$

where ω is the SAW frequency, $\omega = k \cdot v_{SAW}$. Thus, the only unknown parameter A can be determined by using the periodic mass boundary condition[55] of the experimental system and the eigenvectors l_i and U_i can be obtained by solving Eqs. (7)–(9).[50] The stiffness C_{11} is thereby determined to be 285 GPa, and the longitudinal velocity in the [100] direction, calculated by $v_{LA} = \sqrt{\frac{C_{11}}{\rho}}$, is 7390 m/s.

Therefore, all the stiffnesses of BAs were measured as $C_{11} = 285$ GPa, $C_{12} = 79.5$ GPa, and $C_{44} = 149$ GPa. The elastic modulus of an arbitrary direction is determined from the elastic compliances (S_{ij}),[56]

$$E_{hkl} = \frac{1}{S_{11} - 2(S_{11} - S_{12} - 0.5S_{11})(a_1^2 a_2^2 + a_2^2 a_3^2 + a_3^2 a_1^2)}, \tag{10}$$

where ⟨hkl⟩ is the Miller index and a_1, a_2, and a_3 are directional cosines. Hence, E_{100}, E_{110}, and E_{111} are 250, 308, and 335 GPa, respectively. In addition, Poisson's ratio of BAs, determined similar to Eq. (10), is[56]

$$\nu_{ab} = -\frac{S_{12} + (S_{11} - S_{12} - 0.5S_{44})\left(e_1^2 b_1^2 + e_2^2 b_2^2 + e_3^2 b_3^2\right)}{S_{11} - 2(S_{11} - S_{12} - 0.5S_{44})(e_1^2 e_2^2 + e_2^2 e_3^2 + e_3^2 e_1^2)}, \tag{11}$$

where e_i and b_i are directional cosines of the transversal and axial strain. Poisson's ratio in the ⟨100⟩ direction on the (100) plane was measured as 0.22. Additionally, the averaged elastic (E_{VRH}) and shear moduli (G_{VRH}) of BAs can be determined by the Voigt-Reuss-Hill average method,[57]

$$E_{VRH} = \frac{1}{2}\left(\frac{(C_{11} - C_{12} + 3C_{44})(C_{11} + 3C_{12})}{2C_{11} + 3C_{12} + C_{44}} + \frac{5}{3S_{11} + 2S_{12} + S_{44}}\right), \tag{12}$$

$$G_{VRH} = \frac{1}{2}\left(\left(\frac{C_{11} - C_{12} + 3C_{44}}{5}\right) + \left(\frac{5}{4(S_{11} - S_{12}) + 3S_{44}}\right)\right). \tag{13}$$

The averaged elastic and shear moduli were measured as 326 and 128 GPa, respectively. Despite a lower sound velocity, it should be noted that E_{VRH} is about twice as high as that of silicon (~160 GPa) and comparable to that of GaN (~300 GPa), due to the large mass density. This result suggests that BAs is a good mechanical material for micromachining and high pressure applications.

To analyze the experimental results, we applied *ab initio* theory to calculate the mechanical properties of BAs including the bulk modulus, elastic modulus, and Poisson's ratio. We applied the density functional theory (DFT) to calculate the force acting on each atom using the Quantum ESPRESSO package.[58,59] We used projection-

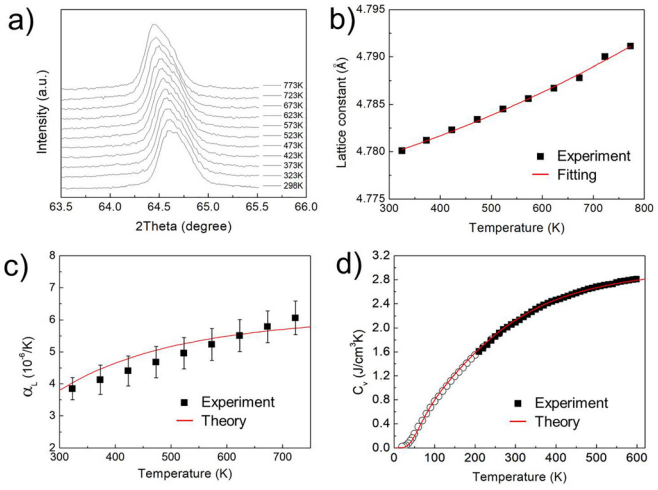

FIG. 4. Thermal properties of BAs. (a) The temperature dependent X-ray diffraction (XRD) measurement for (311) peaks with temperatures from 298 K to 773 K; (b) the measured lattice constant of BAs as a function of temperature. The red line represents the second order polynomial fitting; (c) the linear thermal expansion coefficient (α_L) of BAs with temperature dependence; and (d) the specific heat (C_v) of BAs from 5 to 600 K. Symbols indicate experimental data, and the red line represents the DFT calculations.

augmented wave pseudopotentials under local density approximation for both boron and arsenic.[60] An 8 atom unit cell with $6 \times 6 \times 6$ Monkhorst-Pack k-point meshes is used for relaxation, and the relaxed lattice constant for BAs is 4.7434 Angstrom. We expand the lattice constants by 0.001 Angstrom and calculate the pressure applied on the unit cell by DFT. The calculated bulk modulus, C_{11}, C_{12}, C_{44}, and Poison's ratio ($\langle 100 \rangle$) are 150 GPa, 294 GPa, 80.6 GPa, 177 GPa, and 0.22, respectively, in good agreement with experiments.

We also measured the thermal expansion coefficients of BAs by temperature dependent X-ray diffraction (XRD) using a Cu Kα radiation source. Figure 4(a) shows the XRD data from 293 to 773 K. As the temperature increases, the (311) peak clearly shifts to a smaller angle [Fig. 4(a)], indicating an increase in the lattice constant. The measured lattice constant of BAs at 298 K is 4.78 Å and agrees with our previous report.[7] The temperature-dependent lattice constants (l) of BAs [Fig. 4(b)] were used to obtain the linear thermal expansion coefficient (α_L),

$$\alpha_L \equiv \frac{1}{l}\frac{dl}{dT}. \tag{14}$$

The measured α_L (T) is fit using the least squares method with a second-order polynomial curve [Fig. 4(b) to obtain the thermal expansion coefficient in Fig. 4c: α_L is 3.85×10^{-6}/K at 298 K and increases to 6.06×10^{-6}/K at 723 K. Due to its cubic structure, BAs has a volumetric thermal expansion $\alpha_v = 3 \cdot \alpha_L = 11.55 \times 10^{-6}$/K at room temperature. Here, we also performed *ab initio* calculations of the thermal expansion.[63–65] The thermal expansion coefficient can be calculated from phonon dispersion and mode Gruneisen parameters. The phonon dispersion is calculated from the 2nd order interatomic force constants (IFCs), and Grüneisen parameters are calculated from the 2nd and 3rd order IFCs using the ALAMODE package[66] based on the 216 atom supercell using the finite displacement plus least squares fitting method. Our measurement results show good agreement with the calculation [Fig. 4(c)] and recent study.[61,62]

Knowledge of the thermal expansion property of BAs is critical for its integration into high-power electronics materials to take advantage of the ultrahigh thermal conductivity. A thermal expansion match between device layers is desired to minimize the residual stress and prevent the delamination of materials with their adjacent layers, as well as to reduce the thermal boundary resistance.[67] Therefore, it is worthy to compare α_L of BAs with those of GaN and GaAs, as they are potential target materials for passive cooling applications of BAs. α_L of GaN is 3.94×10^{-6}/K at 300 K and 5.33×10^{-6}/K at 800 K (a-axis)[68] and that of GaAs is 5.9×10^{-6}/K at 300 K.[69] These values are close to our measured thermal expansion coefficients of BAs, thereby underscoring the high promise of BAs as a superior cooling material for high power and high frequency GaN or GaAs electronic devices. In comparison, those prototype high thermal conductivity materials, diamond (1.6×10^{-6}/K)[70] and SiC (3.2×10^{-6}/K)[71] at room temperature, have a much larger thermal expansion mismatch that can potentially lead to thermal mechanical instability and large thermal boundary resistances.

We also measured the temperature dependent specific heat (C_v) of BAs using differential scanning calorimetry in Fig. 4(d). In addition,

TABLE I. Summary of experimentally measured physical properties of BAs.

Physical property	Experimental value	References
Crystal structure	Zinc-blende cubic ($F\bar{4}3m$)	Refs. 7–9 and 18
Lattice constant (Å)	4.78	Refs. 7 and 18
Bandgap (eV)	1.82	This work
Refractive index	3.29 (657 nm) 3.04 (908 nm)	This work
Mass density (g/cm^3)	5.22	Refs. 7 and 18
Stiffness C_{11}, C_{12}, C_{44} (GPa)	285, 79.5, 149	This work
Compliance S_{11}, S_{12}, S_{44} ($\times 10^{-12}$ Pa^{-1})	3.99, −0.87, 6.71	This work
Averaged elastic modulus (GPa)	326	This work
Averaged shear modulus (GPa)	128	This work
Bulk modulus (GPa)	148	Ref. 47
Poisson's ratio	0.22 ($\langle 100 \rangle$ on (100))	This work
Longitudinal sound velocity (m/s)	7390 ($\langle 100 \rangle$) 8150 ($\langle 111 \rangle$)	This work
Transverse sound velocity (m/s)	5340 ($\langle 100 \rangle$)	This work
Thermal conductivity (W/m·K)	1300	Ref. 7
Volumetric heat capacity (J/cm^3 K)	2.09	This work, Refs. 7 and 73
Thermal expansion coefficient (10^{-6} K^{-1})	3.85 (linear) 11.55 (volume)	This work
Grüneisen parameter	0.82	This work

we performed *ab initio* calculations[72] using the same DFT settings. When plotted together, our experimental data from this work (solid squares) and prior work[7,73] (open circles) show good agreement with the theory [Fig. 4(d)]. Moreover, the Grüneisen parameter (γ)[74] is generally used to describe the effect of the volumetric change of a crystal on the vibrational properties and is a weighted average over all phonon modes[45] and can be calculated by

$$\gamma = \frac{\alpha_v B}{C_v}, \tag{15}$$

where α_v and C_v are the volume expansion coefficient and specific heat capacity, respectively. In our study, the room temperature Grüneisen parameter of BAs was determined as $\gamma = 0.82$.

In summary, we report systematic experimental measurements of important physical properties of cubic BAs, including the bandgap, refractive index, elastic modulus, shear modulus, Poisson's ratio, thermal expansion coefficient, and specific heat capacity. The database of the physical properties of BAs, with the room temperature values summarized in Table I, is now complete after addition of the experimental values from this work to the literature. With an ultrahigh thermal conductivity of 1300 W/mK,[7] we believe that the systematically reported physical properties of BAs will further facilitate the development of this new semiconductor for thermal, electrical, optical, and mechanical applications.

Y. H. acknowledges support from a CAREER award from the National Science Foundation under Grant No. DMR-1753393, an Alfred P. Sloan Research Fellowship under Grant No. FG-2019-11788, a Young Investigator Award from the U.S. Air Force Office of Scientific Research under Grant No. FA9550-17-1-0149, a Doctoral New Investigator Award from the American Chemical Society Petroleum Research Fund under Grant No. 58206-DNI5, and the UCLA Sustainable LA Grand Challenge and the Anthony and Jeanne Pritzker Family Foundation.

REFERENCES

[1]M. M. Waldrop, Nature **530**, 144 (2016).
[2]P. Ball, Nature **492**, 174 (2012).
[3]S. Chu and A. Majumdar, Nature **488**, 294 (2012).
[4]A. Shehabi *et al.*, United States Data Center Energy Usage Report No. LBNL-1005775 (2016).
[5]International Technology Roadmap for Semiconductors, ITRS 2.0 2015 edition; www.itrs2.net/. (2015).
[6]J. S. Kang, H. Wu, and Y. Hu, Nano Lett. **17**, 7507 (2017).
[7]J. S. Kang, M. Li, H. Wu, H. Nguyen, and Y. Hu, Science **361**, 575 (2018).
[8]S. Li *et al.*, Science **361**, 579 (2018).
[9]F. Tian *et al.*, Science **362**, 582 (2018).
[10]A. Sood *et al.*, in *Proceedings of the 17th Intersociety Conference Thermal Thermomechanical Phenomena in Electronic Systems* (IEEE, 2018), p. 1396.
[11]A. Bar-Cohen and P. Wang, J. Heat Transfer **134**, 051017 (2012).
[12]Y. Won *et al.*, IEEE Trans. Compon., Packag. Manufacuring Technol. **5**, 737 (2015).
[13]*Handbook of Crystal Growth—Vol. II: Bulk Crystal Growth*, edited by T. Nishinaga and P. Rudolph (Elsevier, Amsterdam, 2015).
[14]A. M. Marconnet *et al.*, Rev. Mod. Phys. **85**, 1295 (2013).
[15]L. Lindsay, D. A. Broido, and T. L. Reinecke, Phys. Rev. Lett. **111**, 25901 (2013).
[16]T. Feng, L. Lindsay, and X. Ruan, Phys. Rev. B **96**, 161201(R) (2017).
[17]H. Fan, H. Wu, L. Lindsay, and Y. Hu, Phys. Rev. B **100**, 085420 (2019).
[18]J. A. Perri, S. Laplaca, and B. Post, Acta Crystallogr. **11**, 310 (1958).
[19]F. V. Williams and R. A. Ruehrwein, J. Am. Chem. Soc. **82**, 1330 (1960).
[20]J. Osugi, K. Shimizu, and Y. Tanaka, Proc. Jpn. Acad. **42**, 48 (1966).
[21]S. M. Ku, J. Electrochem. Soc. **113**, 813 (1966).
[22]A. F. Armington, J. Cryst. Growth **1**, 47 (1967).
[23]T. L. Chu and A. E. Hyslop, J. Appl. Phys. **43**, 276 (1972).
[24]D. J. Stukel, Phys. Rev. B **1**, 3458 (1970).
[25]C. Prasad and M. Sahay, Phys. Status Solidi **154**, 201 (1989).
[26]M. P. Surh, S. G. Louie, and M. L. Cohen, Phys. Rev. B **43**, 9126 (1991).
[27]G. L. W. Hart and A. Zunger, Phys. Rev. B **62**, 13522 (2000).
[28]K. Bushick *et al.*, Appl. Phys. Lett. **114**, 022101 (2019).
[29]Y. Ge, W. Wan, X. Guo, and Y. Liu, e-print arXiv:1901.03947 (2019).
[30]J. Buckeridge and D. O. Scanlon, Phys. Rev. Mater. **3**, 51601 (2019).
[31]M. Fox, *Optical Properties of Solids* (Oxford University Press, 2004).
[32]I. Bravic and B. Monserrat, e-print arXiv:1904.11511 (2019).
[33]M. Guemou *et al.*, Physica B **407**, 1292 (2012).
[34]J. C. Manifacier, J. Gasiot, and J. P. Fillard, J. Phys. E **9**, 1002 (1976).
[35]B. E. A. Saleh and M. C. Teich, *Fundamentals of Photonics* (John Wiley & Sons, 2019).
[36]W. L. Bond, J. Appl. Phys. **36**, 1674 (1965).
[37]D. T. F. Marple, J. Appl. Phys. **35**, 1241 (1964).
[38]B. A. Auld, *Acoustic Fields and Waves in Solids* (John Wiley & Sons, New York, 1973).
[39]M. A. Hopcroft *et al.*, J. Microelectromech. Syst. **19**, 229 (2010).
[40]O. A. Bauchau and J. I. Craig, *Structural Analysis: With Applications to Aerospace Structures* (Springer Science & Business Media, 2009).
[41]C. Thomsen, H. Grahn, H. Maris, and J. Tauc, Phys. Rev. B **34**, 4129 (1986).
[42]M. Li, J. S. Kang, and Y. Hu, Rev. Sci. Instrum. **89**, 084901 (2018).
[43]J. S. Kang, M. Ke, and Y. Hu, Nano Lett. **17**, 1431 (2017).
[44]Y. Hu, L. Zeng, A. J. Minnich, M. S. Dresselhaus, and G. Chen, Nat. Nanotechnol. **10**, 701 (2015).
[45]J. S. Kang, H. Wu, M. Li, and Y. Hu, Nano Lett. **19**, 4941 (2019).
[46]C. Kittel, *Introduction to Solid State Physics* (Wiley, New York, 1976).
[47]R. G. Greene *et al.*, Phys. Rev. Lett. **73**, 2476 (1994).
[48]F. Tian *et al.*, Appl. Phys. Lett. **114**, 131903 (2019).
[49]L. Rayleigh, Proc. London Math. Soc. **s1**, 4 (1885).
[50]G. W. Farnell, "Properties elastic surface waves," in *Physical Acoustic Principle Methods*, edited W. P. Mason and R. N. Thurst. (Academic, New York, 1970), Vol. VI, pp. 109–166.
[51]Y. Hu, F. Kuemmeth, C. M. Lieber, and C. M. Marcus, Nat. Nanotechnol. **7**, 47 (2012).
[52]J. Rogers, A. Maznev, and K. Nelson, Annu. Rev. Mater. Sci. **30**, 117 (2000).
[53]T. Lee *et al.*, Phys. Rev. B **71**, 144106 (2005).
[54]P. Hess, Phys. Today **55**(3), 42 (2002).
[55]A. A. Maznev and A. G. Every, J. Appl. Phys. **106**, 113531 (2009).
[56]W. A. Brantley, J. Appl. Phys. **44**, 534 (1973).
[57]R. Hill, Proc. Phys. Soc., London, Sect. A **65**, 349 (1952).
[58]P. Giannozzi *et al.*, J. Phys.: Condens. Matter **21**, 395502 (2009).
[59]P. Giannozzi *et al.*, J. Phys.: Condens. Matter **29**, 465901 (2017).
[60]We used the pseudopotentials B.pz-n-kjpaw_psl.0.1.UPF and As.pz-n-kjpaw_psl.0.2.UPF from the Quantum ESPRESSO pseudopotential data base (http://www.quantum-espresso.org/pseudopotentials).
[61]X. Chen *et al.*, e-print arXiv:1903.01668.
[62]S. Li *et al.*, e-print arXiv:1906.04101.
[63]T. H. K. Barron, J. G. Collins, and G. K. White, Adv. Phys. **29**, 609 (1980).
[64]K. Schelling and P. Keblinski, Phys. Rev. B **68**, 035425 (2003).
[65]N. Mounet and N. Marzari, Phys. Rev. B **71**, 205214 (2005).
[66]T. Tadano *et al.*, J. Phys.: Condens. Matter **26**, 225402 (2014).
[67]M. Li, J. S. Kang, H. Nguyen, H. Wu, T. Aoki, and Y. Hu, Adv. Mater. **31**, 1901021 (2019).
[68]R. R. Reeber and K. Wang, J. Mater. Res. **15**, 40 (2000).
[69]J. S. Blakemore, J. Appl. Phys. **53**, R123 (1982).
[70]T. Sato *et al.*, Phys. Rev. B **65**, 092102 (2002).
[71]Z. Li and R. C. Bradt, J. Mater. Sci. **21**, 4366 (1986).
[72]M. Born and K. Huang, *Dyanmical Theory of Crystal Lattices* (Oxford University Press, 1954).
[73]V. I. Koshchenko *et al.*, Inorg. Mater. **17**, 1460 (1981).
[74]E. Grüneisen, Ann. Phys. **344**, 257 (1912).